Recent progress in plasmonic colour filters for image sensor and multispectral applications

Nadia Pinton[a,b], James Grant[b], Bhaskar Choubey[a], David Cumming[b], and Steve Collins[a]

[a]Department of Engineering Science, University of Oxford, Oxford, OX1 3PJ, UK
[b]School of Engineering, University of Glasgow, Glasgow, G12 8LT, UK

ABSTRACT

Using nanostructured thin metal films as colour filters offers several important advantages, in particular high tunability across the entire visible spectrum and some of the infrared region, and also compatibility with conventional CMOS processes. Since 2003, the field of plasmonic colour filters has evolved rapidly and several different designs and materials, or combination of materials, have been proposed and studied. In this paper we present a simulation study for a single-step lithographically patterned multilayer structure able to provide competitive transmission efficiencies above 40% and contemporary FWHM of the order of 30 nm across the visible spectrum. The total thickness of the proposed filters is less than 200 nm and is constant for every wavelength, unlike e.g. resonant cavity-based filters such as Fabry-Perot that require a variable stack of several layers according to the working frequency, and their passband characteristics are entirely controlled by changing the lithographic pattern. It will also be shown that a key to obtaining narrow-band optical response lies in the dielectric environment of a nanostructure and that it is not necessary to have a symmetric structure to ensure good coupling between the SPPs at the top and bottom interfaces. Moreover, an analytical method to evaluate the periodicity, given a specific structure and a desirable working wavelength, will be proposed and its accuracy demonstrated. This method conveniently eliminate the need to optimize the design of a filter numerically, i.e. by running several time-consuming simulations with different periodicities.

Keywords: Plasmonic Colour Filters, Narrow-band Filters, Nanohole Array, Surface Plasmons, Image Sensors, Aluminium, CMOS-compatible

1. INTRODUCTION

Currently, the colour filters used in CMOS image sensors (CISs) are polymer-based materials. Although these materials are widely used they have several disadvantages. In particular, since they require several lithographic steps for each different colour their implementation is costly and impractical for multispectral applications,. Furthermore, they cannot sustain high temperatures and degrade under long exposure to ultraviolet radiation. Most importantly, because the filters characteristics depend upon the properties of the polymer materials, the spectral properties of the filters are not easy to change. An ideal replacement filter technology would be stable, more easily implemented in existing processes used to make CIS and give the designer the ability to control the spectral characteristics of filters.

A promising alternative to the standard polymer-based filter technologies are so-called Plasmonic Colour Filters (PCFs) which are based upon the phenomenon of Extraordinary Optical Transmission (EOT).[1] This phenomenon was first observed in 1998 in the optical transmission properties of periodic arrays of subwavelength holes milled in, otherwise opaque, metallic layers. Unexpectedly, these structures transmitted light at wavelengths much longer than the cut-off wavelength of the holes themselves, with a transmission efficiency that sometimes exceeded the efficiency expected from the normalized area of the holes. It is now understood that this enhancement in transmission results from the active participation of the metallic layer in the transmission process via the resonant interaction of the incident light, diffraction from every hole, and the Surface Plasmon Resonances (SPRs) generated at the metal/dielectric interfaces of a structure. The SPRs that are key to this process consist of resonant oscillations of surface charges that, having an evanescent character, exponentially decay away from the interface where they have been generated. Since the wave vector of these surface waves, $\mathbf{k}_{SPR}$, is larger than the wave vector of the incident electromagnetic waves traveling into vacuum (or a dielectric), additional momentum

Further author information: (Send correspondence to N.P)
N.P.: E-mail: nadia.pinton@eng.ox.ac.uk, Telephone: +44(0)141 330 6814

Nanophotonics VI, edited by David L. Andrews, Jean-Michel Nunzi, Andreas Ostendorf, Proc. of SPIE
Vol. 9884, 988438 · © 2016 SPIE · CCC code: 0277-786X/16/$18 · doi: 10.1117/12.2227754

is required to excite the SPRs. Diffraction from the sharp edges of individual subwavelength holes in a metal layer can provide the extra momentum required to generate SPRs.[2] However, in the case of a periodic array of holes the additional momentum required to observe EOT is provided by the periodicity of the array.

The idea of using PCFs for image sensor applications was first proposed by *Catrysse et al.*[3] in 2003. Despite the relatively low transmission and poor selectivity of these filters this work demonstrated that it is possible to manufacture filters by patterning the metal layers available in a 180-nm complementary metal oxide semiconductor technology. Since 2003, the field of plasmonic colour filters has evolved rapidly and several different designs and materials, or combinations of materials, have been studied. For example, in 2010, *Chen et al.*[4] first reported the integration and characterization of hexagonal aluminium array plasmonic colour filters on top of a CMOS photodiode, while in 2013 *Burgos et al.*[5] integrated a separate primary colour (RGB) plasmonic filter with a CIS and demonstrated imaging. Nonetheless, PCFs have not yet been able to match the performances of standard polymer-based colour filters and thus, despite their advantages, they have still not replaced existing filters in commercial CMOS image sensors.

In this paper, ways to improve the colour discrimination of plasmonic colour filters are investigated by analyzing the dependence of the optical transmission on the structural parameters of the nanostructure and then making incremental choices and variations. The structural parameters of a plasmonic nanohole array, which determine their optical efficiency, are: periodicity, metal thickness, diameter and the choice of both the metal and the dielectric(s). Some previous studies have argued that to enhance the coupling between the top and bottom surfaces of a metallic film, and hence the performance of the PCFs, the structure should be symmetric. However, simulation results will be presented which show that by using two dielectrics to create an asymmetric structure it is possible to create more selective transmission peaks with a higher peak transmission. Moreover, a simple method is proposed which allows a designer to determine the hole periodicity required to obtain maximum transmission at a particular wavelength.

2. EXISTING PLASMONIC COLOUR FILTERS

Table 1 summarises key characteristics of PCFs that have been reported in the past 4 years. Most of these PCFs have been manufactured using aluminium because this is the metal used in CMOS process and the preferred type of filter is evidently the additive one. These results show that the transmission efficiency can be as high as 70%. However, these results also show the apparent inability of the plasmonic filters to be highly selective and in particular the minimum full-width at half-maximum (FWHM) that has been reported is approximately 50 nm.[6]

Table 1: Key characteristics of plasmonic colour filters reported in the past 4 years.
The symbol * indicate that only simulation results have been presented.

Year	Reference	Type of Structure	Type of filters	Optical Efficiency	FWHM
2012 2013	[4,5,7]	150-nm Al Nanoholes Hexagonal pattern	Additive	Blue $\approx$ 55% Green $\approx$ 45% Red $\approx$ 50%	$\approx$ 100 nm $>$ 100 nm $\approx$ 150 nm
2013	[8]	30-nm Ag Nanogratings	Subtractive	Cyan $\approx$ 45% Magenta $\approx 50-60\%$ Yellow $\approx 60-70\%$	n/a n/a n/a
2014	[9]	40-nm Al Nanosquares Squared pattern	Subtractive	Cyan $\approx$ 40% Magenta $\approx 50-60\%$ Yellow $\approx 60-70\%$	n/a n/a n/a
2014*	[6]	MIM and IM Al/Si_3N_4 Nanosquares Square pattern	Additive	Blue $<$ 40% Green $<$ 40% Red $<$ 40%	50 nm 50 nm 50 nm
2015*	[10]	200-nm Al layer Cross-shaped holes Squared pattern	Additive	Blue 25% Green 22.7% Red 17.5%	100 nm 100 nm 100 nm

In order to maintain the compatibility of the filters with standard CMOS processes, the metal of choice is aluminium. Based upon the results in Table 1, and taking into consideration ease of fabrication, in particular the fact that circular

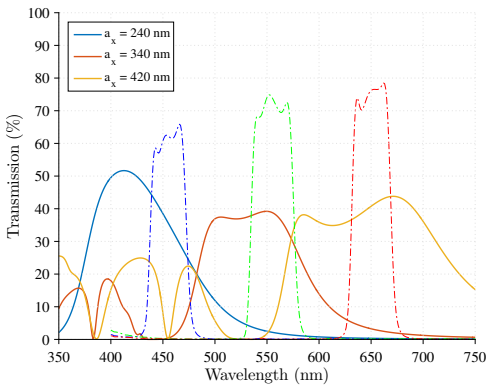

(a) Transmission RGB PCFs

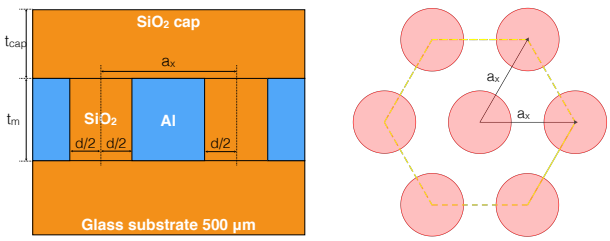

(b) (x, z) cross-sectional and top-down view

Figure 1: (a) Transmission curves of RGB 150-nm Al hexagonal nanohole array surrounded by silicon dioxide, and (b) (x, z) cross-sectional and top-down view of the of the structure. The blue filter is given by an array periodicity a_x of 240 nm and a diameter $d = 140$ nm, while the green and red filters have a_x of 340 nm, $d = 180$ nm and a_x of 420 nm, $d = 280$ nm, respectively. In (a) the dashed curves represent the transmission curve for commercially available Fabry-Perot blue, green and red filters,[11] respectively.

nanoholes are much easier to create than square or cross-shaped holes, the most promising results have been obtained with hexagonal circular nanohole arrays in a 150-nm thick aluminium layer. Fig. 1a shows the simulated transmission coefficient of this type of CMOS-compatible PCFs, when the 150-nm thick aluminium layer is sandwiched between layers of silicon oxide (see Fig. 1b). In particular this figure shows the transmission coefficients of the three filters that have been designed to have transmission peaks in the red, green and blue parts of the spectrum. The ability to vary the wavelength at which maximum transmission occurs that has been used to create these filters arises from the fact that the peak wavelength depends upon the periodicity of the nanohole array. This is because the periodicity of the array provides the additional momentum necessary to observe the EOT phenomenon.[1,4,12]

At a metal/dielectric interface, the SPRs are called Surface Plasmon Polaritons (SPPs). Different from Localized Surface Plasmon Resonances (LSPRs), which can be observed e.g. in nanoparticles, they have a propagating character, parallel to the interface. The SPPs wavevector is given by:

$$\|\mathbf{k}_{\mathrm{SPP}}\| = \|\mathbf{k}_0\| n_{\mathrm{SPP}} = \frac{2\pi f}{c_0} n_{\mathrm{SPP}} = \frac{2\pi}{\lambda} n_{\mathrm{SPP}} = \frac{2\pi}{\lambda_{\mathrm{SPP}}} \quad \text{with} \quad n_{\mathrm{SPP}} = \sqrt{\frac{\epsilon_d \epsilon_m}{\epsilon_d + \epsilon_m}} \tag{1}$$

where ϵ_d and ϵ_m are the the relative permittivity of the dielectric and the metal, respectively, that compose the interface, n_{SPP} is the SPPs refractive index and λ_{SPP} is the SPPs wavelength; f and λ are frequency and wavelength in free space respectively, c_0 is the speed of light and $\mathbf{k}_0$ is the wavevector of the light traveling in free space.

As said previously, the surface plasmon wavevector is larger than the wavevector of light in free space and thus additional momentum is required to generate SPPs. This additional momentum is provided by the periodic nanohole array and it therefore follows that the condition that has to be satisfied to excite SPPs efficiently is:

$$\mathbf{k}_{\mathrm{SPP}} = \mathbf{k}_{\|} + \mathbf{G} \tag{2}$$

where $k_{\|}$ is the component along the direction parallel to the interface of magnitude $k_{\|} = k \sin\theta$, and G is a reciprocal vector given by the periodicity of the array. In case of normal incidence, $\theta = 0 \Rightarrow \mathbf{k}_{\|} = 0$, and thus Eq. 2 becomes:

$$k_{\mathrm{SPP}} = G \tag{3}$$

The additional momentum G is determined by the periodicity of the array, and for a triangular pattern of holes within a hexagonal array of holes with period a_x it is given by:

$$G_{ij} = \frac{4\pi}{a_x \sqrt{3}} \sqrt{i^2 + j^2 + ij} \tag{4}$$

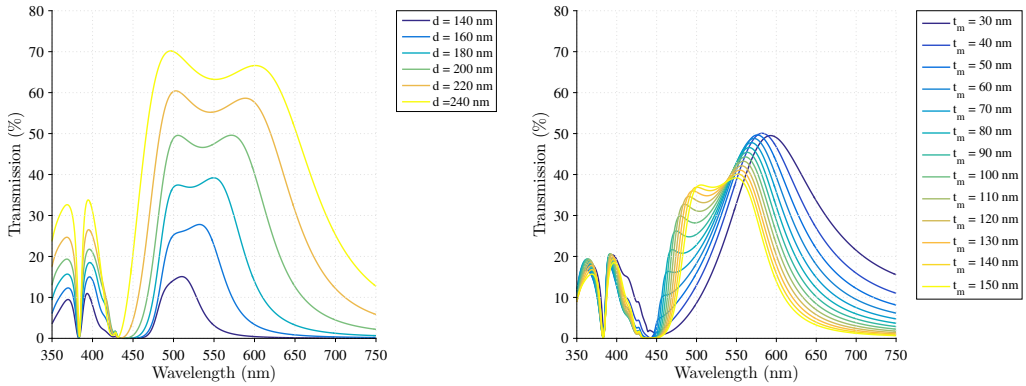

(a) T vs. Diameter **(b)** T vs. Metal thickness

Figure 2: Transmission as a function of (a) diameter and (b) aluminium thickness of the structure depicted in Fig. 1b having periodicity a_x of 340 nm and a diameter d = 180 nm. The diameter does not affect the 'shape' of the curve while accordingly to the value of the metal thickness one peak (thin layers) or two peaks (thicker layers) can be observed.

where i and j are integers (with $i \geq 0$, $j > 0$) and indicate the diffraction orders. It has been observed in several studies that when k_{SPPs} matches the reciprocal vectors G_{ij} of the periodic array, a minima in transmission appears which coincides with the appearance of EOT peaks, but is red-shifted in wavelength. Thus, by combining Eqs. 3 and 4 it is possible to predict at which wavelengths the transmission minima occurs. The wavelengths λ_{min} at which the transmission minima are predicted to occur are given by:

$$(\lambda_{\mathrm{min}})_{ij} = \frac{\sqrt{3}}{2\sqrt{i^2 + j^2 + ij}} n_{\mathrm{SPP}} a_x \tag{5}$$

In addition to the transmission characteristics of three PCFs, Fig. 1a also shows the transmission characteristics of a commercial type of Fabry-Perot RGB filters.[11] A comparison of these characteristics shows that the main drawback of these PCFs is relatively low peak transmission and the comparatively large bandwidth of these filters. As previously already reported,[13] the diameter of the nanoholes does not affect the shape of the pass-band filter but increasing the diameter of the holes increases the transmission efficiency (see Fig. 2a). However, as these results show increasing the diameter of the nanoholes also increases the bandwidth of the filter. An alternative approach to increase the peak transmission is to reduce the thickness of the metal layer.[13] Fig. 2b shows that reducing the metal film thickness increases the maximum transmission efficient. In addition, these results show that it is possible to obtain a single peak in transmission by reducing the thickness of the aluminium layer between 30 nm and 50 nm.

3. SIMULATION RESULTS TOWARDS NARROW-BAND PLASMONIC COLOUR FILTERS

All the simulations have been carried out with the Lumerical FDTD Solutions software. A broadband light source normally incident on the x-y plane and electrically polarized along the x-direction (TM polarization with respect the x axis) has been utilized. To reduce the simulation time a single unit cell of the periodic array under study have been modelled, and symmetric/antisymmetric boundary conditions have been used, consistently with the source polarization. The total transmission spectra have been recorded with DFT Monitors, perpendicular to the direction of propagation of light (z direction), placed in front of the source, at the top of the structures, within the simulation volume defined. A finer mesh region has been introduced at the holes level to improve the accuracy, having a maximum mesh step of 5 nm. Aluminium and silicon dioxide have been modelled with the sampled data present within the Lumerical material database as "Al (Aluminium) - Palik" and "SiO2 (Glass) - Palik", respectively.

Even though using a thin metal layer does not reduce the bandwidth of the filter the presence of a single peak in transmission is a promising starting point for the development of better PCFs. The starting point for a new filter design that has been selected is therefore a 40 nm thick aluminium layer, which is between two and three times the penetration depth of the SPPs in the aluminium (see Appendix A). This thickness should therefore ensure that the film is not so thin that

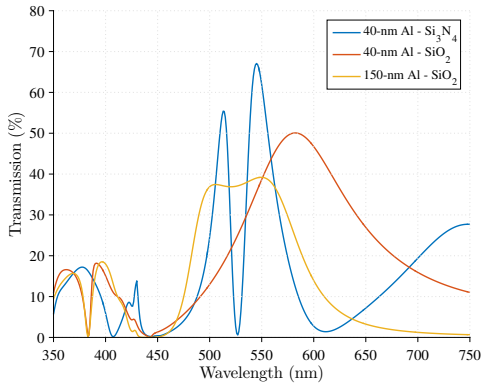

Figure 3: (a) Transmission of a 40-nm Al hexagonal nanohole array onto a glass substrate in a silicon nitride environment in comparison with the simulated transmission efficiency of the same nanohole array with silicon dioxide hole fill and cap and the same filter design in a thicker aluminium layer also filled and capped with silicon dioxide, having the same periodicity a_x of 340 nm and a diameter d = 180 nm.

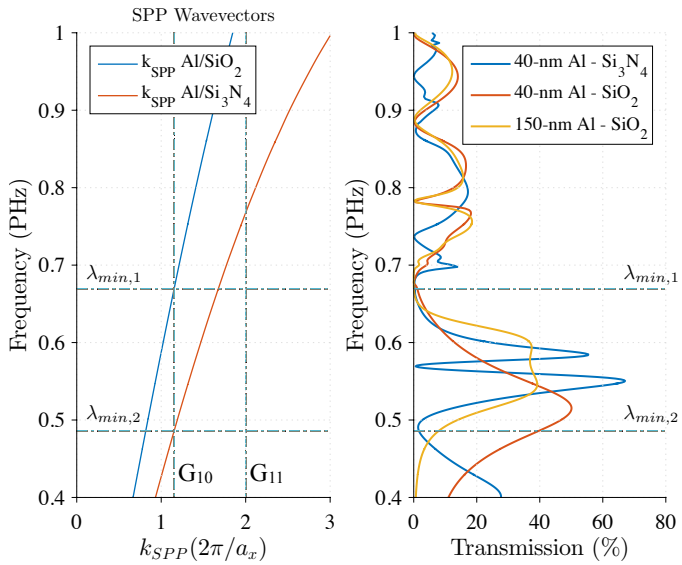

Figure 4: (left) SPPs wave vectors at the Al/SiO_2 and Al/Si_3N_4 interfaces and (right) Transmission curves vs. Frequency, to display the relationship between minima in transmission, periodicity and additional momenta. Minima appears when $k_{SPP} = G_{ij}$

the top and bottom interfaces couple through the metal and split the surface plasmon resonances of the aluminium-silicon dioxide interfaces into symmetric and asymmetric modes.

3.1 Dielectric environment

Since the choice of metal has been pre-selected in order to ensure the compatibility of the structure with conventional CMOS process, the only parameter that has not been considered previously is what has been referred to as the 'dielectric environment' of the metal film and the nanohole array, i.e. the dielectric substrate and dielectric layer that caps the structure. For ease of fabrication and characterization of the filters, the substrate will be assumed to be silicon dioxide. This means that the two remaining variables are the dielectric inside the nanoholes and on top of the nanostructure. There are many choices of dielectrics, but only a few, including aluminium oxide and silicon nitride, are both not-absorbing in the visible and CMOS-compatible. Since silicon nitride is the common cap layer for CMOS image sensors this is a sensible choice of capping layer.

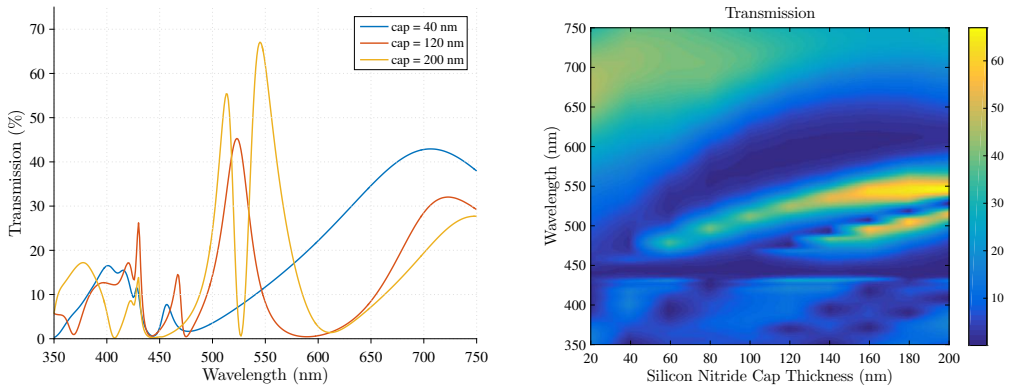

(a) T vs. Cap thickness. **(b)** T vs. Wavelength vs. Cap thickness.

Figure 5: (a) Transmission of the 40-nm Al structure as a function of the silicon nitride cap thickness, and (b) transmission vs. wavelength vs. silicon nitride cap layer thickness.

Fig. 3 shows the simulated transmission efficiency of a hexagonal nanohole array in a 40-nm aluminium layer, on top of a silicon dioxide substrate, with holes filled with silicon nitride and all covered by a 200 nm silicon nitride cap. For comparison this figure also shows the simulated transmission efficiency of the same nanohole array with silicon dioxide hole fill and cap and the same filter design in a thicker aluminium layer also filled and capped with silicon dioxide. Unexpectedly, the use of the silicon nitride capping layer creates two well-separated peaks, with FWHM of aprroximately 50 nm and 20 nm respectively. Silicon nitride (Si3N4), not being a default material in Lumerical, has been added to the software database by creating a new *Sampled data* material and by inserting its (n,k) values, obtained from the tool *PhotonicsDB: Optical Constants*.[14]

Accord to equation (5), the introduction of the silicon nitride on top of the top aluminium surface will provide a different additional momentum than the bottom aluminium-silicon dioxide interface provides. It will therefore create a new plasmonic resonance given by the aluminium-silicon nitride interface. Fig. 4 shows the relationship between minima in transmission, periodicity and additional momenta. In particular the condition $k_{SPP} = G_{10}$, for the Al/SiO_2 and Al/Si_3N_4 interfaces each correspond to a different minimum in transmission ($\lambda_{min,1}$ and $\lambda_{min,2}$ respectively). These two minima therefore appear to relate to the momentum that can be added by the different SPPs. However, this mechanism does not explain the presence of the minimum in transmission at around 530 nm.

Changing the capping dielectric has a potentially positive effect on the transmission characteristics of the filter. However, the two transmission peaks generated by the 200nm cap are not ideal. Figs. 5a and 5b therefore show the dependence of the filter's transmission on the thickness of the silicon nitride cap layer. As highlighted in Fig. 5b, as the cap thickness decreases both the maximum peaks blue-shift in wavelength until the shorter wavelength peak coincides with the transmission minimum at 440 nm. Once this has happened the filter has a single and selective transmission peak having a FWHM of 30 nm and a transmission efficiency above 40%.

The use of a different capping dielectric, and in particular the thickness of this cap, introduces a new design parameter that has a significant impact of the response of a PCF. In particular, if the cap is'too thick' there are two resonant peaks in transmission whilst if the layer is 'too thin' both narrow peaks disappear to leave a single broad transmission peak. According to Fig. 5b, for wavelengths corresponding to green light (520-550 nm), a silicon nitride cap layer of 90-100 nm results in a single, narrow transmission peak.

Again, accordingly to Eq. (5), it is possible to change the wavelength at which the narrow peak occurs by changing the periodicity of the nanohole array. Fig. 6 shows the simulated optical transmission for three different periodicities a_x of the 40-nm Al filters, having silicon nitride filling inside the holes and 100 nm silicon nitride cap layer. For comparison this figure also shows the 150-nm thick Al PCFs (dashed curves) presented at the beginning of the section, of the same three periodicities. The structure with the smallest periodicity has a short-wavelength transmission peak at around 350 nm that, when compared to Fig. 5a, suggests that filters for shorter wavelength would ideally require a slightly thinner silicon nitride layer. However, this second peak falls outside the wavelength range that is often used to define the visible range of wavelengths and hence it appears that a 100-nm thick cap is a good choice for visible wavelengths.

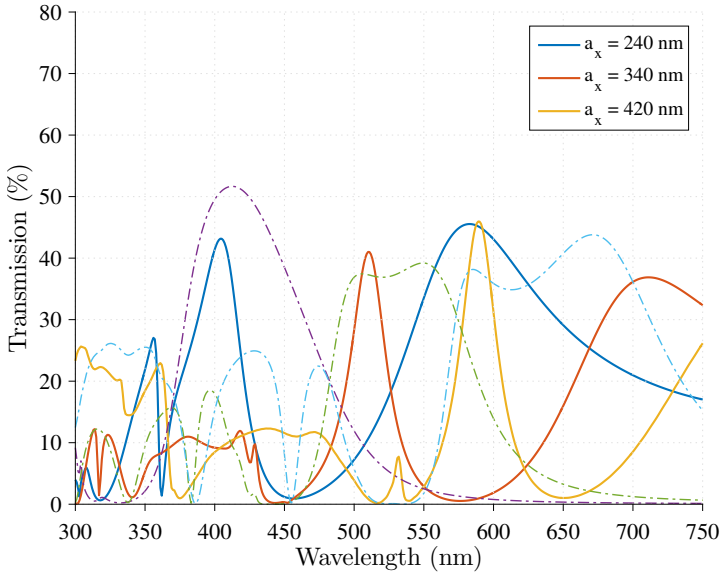

Figure 6: Comparison of the optical transmission of the 40-nm Al filters, having silicon nitride filling inside the holes and 100 nm silicon nitride cap layer, with the RGB 150-nm thick Al PCFs (dashed curves). Periodicities a_x = 240 nm, 340 nm and 420 nm, and diameters d of 140 nm, 180 nm and 240 nm respectively.

An important observation from Fig. 6 is that the peak transmissions of the three new filter designs are comparable to the peak transmissions of the previous design. However, the new filter designs exhibit significantly narrower transmission peaks, in particular they have FWHM of 43 nm (a_x = 240 nm), 30 nm (a_x = 340 nm) and 30 nm (a_x = 420 nm), i.e. their widths are approximately one third of the widths of the 150-nm filters of the same periodicity. The only limitation with these new designs is that each of them has a broad transmission peak at a wavelength that is 1.5 times longer than the wavelength of the narrow-band resonant peak (noticeable clearly in the 240-nm periodicity curve).

To the best of our knowledge the theory of SPPs for nanohole arrays only provides an estimate of the position of a transmission peak based upon the observation that this is at a longer wavelength than a predictable minimum in transmission. From Fig. 6, it can be observed that the narrow peaks don't quite reach their maximum at the required wavelengths, which in this case are at 450 nm, 550 and 650 nm respectively. To avoid the need to optimize the design of a filter numerically, i.e. by running several time-consuming simulations with different periodicities, it would be convenient to have a more accurate method of relating the wavelength of maximum transmission and the periodicity of the nanohole array.

To start, assume a 40-nm Al film with holes filled with silicon nitride and a 100-nm thick silicon nitride cap layer. In the following, an accurate method for the evaluation of the periodicity, for this specific structure and given the wavelength at which it is desirable for the narrow peak to occur, will be provided. For this structure, the narrow transmission peak occurs between two minima, $\lambda_{\min,1}$ and at $\lambda_{\min,2}$, that each appear to be associated with the SPPs on one of the two interfaces accordingly to:

$$k_{\mathrm{SPP},Al/SiO_2}(\lambda_{\min,1}) = G_{10} = \frac{4\pi}{\sqrt{3}a_x}$$
$$k_{\mathrm{SPP},Al/Si_3N_4}(\lambda_{\min,2}) = G_{10} = \frac{4\pi}{\sqrt{3}a_x}$$

The above theoretical minima, though, do not always match the simulated minima $\tilde{\lambda}_{\min,1}$, $\tilde{\lambda}_{\min,2}$ (see Table 2). Two possible explanations are:

- The formula for the wave vectors of the SPPs, even though being a good approximation, does not take into consideration the presence of the holes at the interface. In fact, it could be noticed in Fig. 2a that, even in the case of 150-nm thick Al layer, the minimum $\lambda_{\min,1}$ undergoes a slight blue shift in wavelength as the diameter's size increases. More specifically, the smaller the periodicity to diameter ratio the larger the blue-shift.

- The formula for the wave vectors of the SPPs is designed for an interface between semi-infinite materials (such as for the case of a semi-infinite glass substrate in the simulations) and therefore only an approximation for very thin film layers. This statement is supported by the observation that the second minima $\lambda_{\text{min},2}$ appears to converge to its theoretical value as the thickness of the silicon nitride cap layer approaches twice the penetration depth of the top surface's SPPs into the silicon nitride capping layer. (See Fig. 5b).

These explanations mean that first it is necessary to replace the theoretical values for the SPPs wavevectors with new approximations, that will be indicated as ${}^*k_{\text{SPP},Al/SiO_2}$ and ${}^*k_{\text{SPP},Al/Si_3N_4}$. These have been obtained from the observed positions of minima, $\tilde{\lambda}_{\text{min},1}$ and $\tilde{\lambda}_{\text{min},2}$, in the three simulations run so far, listed in Table 2 together with their relative variations $\Delta\lambda$. The new approximations are listed in Table 3.

Table 2: List of the theoretical and simulated values $k_{\text{SPP},Al/SiO_2}|_{\lambda_{\text{min},1}} = G_{10}$, $k_{\text{SPP},Al/Si_3N_4}|_{\lambda_{\text{min},2}} = G_{10}$, and $k_{\text{SPP},Al/SiO_2}|_{\tilde{\lambda}_{\text{min},1}} = G_{10}$, $k_{\text{SPP},Al/Si_3N_4}|_{\tilde{\lambda}_{\text{min},2}} = G_{10}$ respectively; the simulated λ_{peak} at which the maximum narrow peak occur and the relative $\Delta\lambda = x \cdot \lambda$ for the three periodicities a_x.

Structural param. (nm)	$\lambda_{\text{min},1}$ (nm)	$\tilde{\lambda}_{\text{min},1}$ (nm)	$\Delta\lambda_1$	$\lambda_{\text{min},2}$ (nm)	$\tilde{\lambda}_{\text{min},2}$ (nm)	$\Delta\lambda_2$	λ_{peak} (nm)
$a_x = 240$, $d = 140$	330	318	≈ -3.7%	457	457	0	404
$a_x = 340$, $d = 180$	448	443	≈ -1.1%	616	576	≈ -6.5%	510
$a_x = 420$, $d = 240$	544	535	≈ -1.7%	748	650	≈ -13%	590

Table 3: New approximations for the SPPs wavevectors.

${}^*k_{\text{SPP},Al/SiO_2}(\lambda) = k_{\text{SPP},Al/SiO_2}(\lambda) - k_{\text{SPP},Al/SiO_2}(\lambda)/99$
${}^*k_{\text{SPP},Al/Si_3N_4}(\lambda) = k_{\text{SPP},Al/Si_3N_4}(\lambda) - \Delta k(\lambda - \tilde{\lambda}_{\text{min},2}) k_{\text{SPP},Al/Si_3N_4}(\lambda - \tilde{\lambda}_{\text{min},2}\|_{a_x=240})$ where $\Delta k = 0.00068$

The observation that smaller periodicity to diameter ratios cause larger blue-shifts in the position of a transmission minimum means that the different periodicity to diameter ratios of the different filters will cause the variations $\Delta\lambda_1$ to differ for each filter. Assuming an even reduction in wavelength $\Delta\lambda = 1\%\lambda$, the ${}^*k_{\text{SPP},Al/SiO_2}$ has been evaluated as follow:

$$
\begin{aligned}
{}^*k_{\text{SPP},Al/SiO_2}(\tilde{\lambda}_{\text{min},1}) = k_{\text{SPP},Al/SiO_2}(\lambda_{\text{min},1}) = G_{10} = k_{\text{SPP},Al/SiO_2}(\tilde{\lambda}_{\text{min},1}) - \Delta k \\
\implies \Delta k = k_{\text{SPP},Al/SiO_2}(\tilde{\lambda}_{\text{min},1}) - k_{\text{SPP},Al/SiO_2}(\lambda_{\text{min},1}) = \\
= \frac{2\pi}{\tilde{\lambda}_{\text{min},1}} n_{\text{SPP},Al/SiO_2} - \frac{2\pi}{\lambda_{\text{min},1}} n_{\text{SPP},Al/SiO_2} = \\
= \frac{2\pi}{\lambda_{\text{min},1} - \Delta\lambda} n_{\text{SPP},Al/SiO_2} - \frac{2\pi}{\lambda_{\text{min},1}} n_{\text{SPP},Al/SiO_2} = \\
= \frac{2\pi}{\lambda_{\text{min},1}} n_{\text{SPP},Al/SiO_2} \left(\frac{1}{0.99} - 1 \right) \\
\implies \Delta k(\lambda) = \frac{1}{99} k_{\text{SPP},Al/SiO_2}(\lambda) \qquad \forall\lambda \\
\implies {}^*k_{\text{SPP},Al/SiO_2}(\lambda) = k_{\text{SPP},Al/SiO_2}(\lambda) - k_{\text{SPP},Al/SiO_2}(\lambda)/99
\end{aligned}
$$

Note that to ensure the accuracy of the proposed method the user should utilize a fixed periodicity to diameter ratio of 1.8 for the size of the diameter, once evaluated the periodicity. The user should also take notice that in this case a decrease in wavelength results in a decrease of the new wavevector. This might be counterintuitive at first, but this is due to the fact that the additional momentum is fixed and thus to compensate for the increment in wavevector consequent to a decrease of wavelength it is necessary to introduce a Δk downshift.

From Table 2 it is possible to evaluate a proportional decrement Δk per nanometer for the theorical wavevector $k_{\mathrm{SPP},Al/Si_3N_4}$. For a periodicity $a_x = 240$ nm, $k_{\mathrm{SPP},Al/Si_3N_4}$ and $^*k_{\mathrm{SPP},Al/Si_3N_4}$ coincides. A 100-nm shift in periodicity gives a difference in wavelength $\Delta\lambda_2$ of 6.5%, while a 120-nm shift equals a $\Delta\lambda_2$ of $\approx 13\%$, i.e. a decrement Δk per nanometer of 0.00065 and 0.00072 respectively. It has been chosen a Δk of 0.00068, given by the averages of the two.

At this point, it is possible to evaluate a wavevector $k_{\mathrm{max,avg}}$ for the narrow-band peak. Given that for $a_x = 340$, structural parameter for which the 40-nm silicon nitride structure has been optimized, the maximum peak is found to be exactly at half way between the two minima $\tilde{\lambda}_{\mathrm{min},1}$ and $\tilde{\lambda}_{\mathrm{min},2}$, it follows that:

$$\tilde{\lambda}_{max} = \frac{\tilde{\lambda}_{\mathrm{min},2} + \tilde{\lambda}_{\mathrm{min},1}}{2} =$$
$$= \frac{1}{2}\left(\frac{2\pi}{^*k_{\mathrm{SPP},Al/Si_3N_4}(\tilde{\lambda}_{\mathrm{min},2})} + \frac{2\pi}{^*k_{\mathrm{SPP},Al/SiO_2}(\tilde{\lambda}_{\mathrm{min},1})}\right) = \frac{2\pi}{k_{\mathrm{max,avg}}(\tilde{\lambda}_{\mathrm{max}})}$$
$$\implies \qquad k_{\mathrm{max,avg}}(\lambda) = 2\frac{^*k_{\mathrm{SPP},Al/SiO_2}(\lambda)\,^*k_{\mathrm{SPP},Al/Si_3N_4}(\lambda)}{^*k_{\mathrm{SPP},Al/SiO_2}(\lambda) + ^*k_{\mathrm{SPP},Al/Si_3N_4}(\lambda)} \qquad \forall\lambda$$

Finally, it is necessary to introduce a shift due to the thickness of the silicon nitride layer and thus evaluate a new and last wavevector, called $^*k_{\mathrm{max,avg}}$. In fact, it has been noticed that for example when the silicon nitride goes above a specific threshold value (in this case $t_{\mathrm{cap}} = 100$ nm), the appearance of a second peak 'pushes' the first peak towards longer wavelength, while below the threshold value the peak is not perfectly in the middle of the two minima but it is instead slightly blue-shifted in wavelength. The shift in wavelength has been evaluated as 0.1 nm per nanometer, thus the final formula for the wavevector of the maximum is derived from:

$$^*\lambda_{\mathrm{max,avg}}(\lambda) = \frac{2\pi}{k_{\mathrm{max,avg}}(\lambda)} - 0.1(\lambda - \lambda_{\mathrm{peak}}|_{a_x=340}) \tag{6}$$

In Fig. 7 are plotted all the wavevectors, theoretical and approximations. This graph makes possible to estimate the periodicity given a specific value in wavelength for the maximum peak. For example, if it is required to have a peak at 450 nm:

$$^*k_{\mathrm{max,avg}}(\lambda = 450nm) = G_{10} = \frac{4\pi}{\sqrt{(}3)a_x}$$
$$\implies a_x = \frac{4\pi}{\sqrt{(}3)^*k_{\mathrm{max,avg}}(\lambda = 450nm)}$$

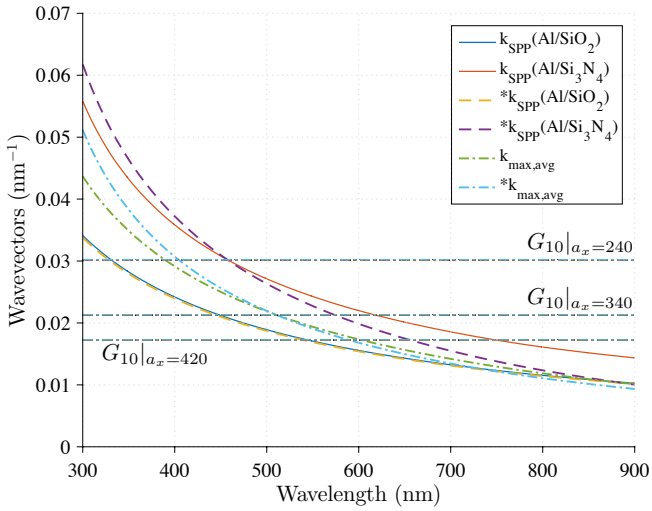

Figure 7: Plot of the theoretical and of the evaluated approximations for the SPPs at the bottom Al/SiO_2 and top Al/Si_3N_4 interface as a function of the wavelength in free space. The * indicate that the wavevector has been subjected to an up/downshift.

Fig. 8 displays the curve simulated with the periodicity values extract from the graph as explained. The accuracy with which the wavelengths for the maximum peaks have been aimed is precise almost at the nanometer.

Unfortunately there is still a conspicuous amount of cross-talk of the blue filter in the red region. It might be noticed though that the curve for the blue filter displays very promising feature for a subtractive colour filter, such as magenta. The technique presented could also be used to evaluate the position of the minima, e.g. the second minima, in order to have zero transmission for specific colour of the spectrum.

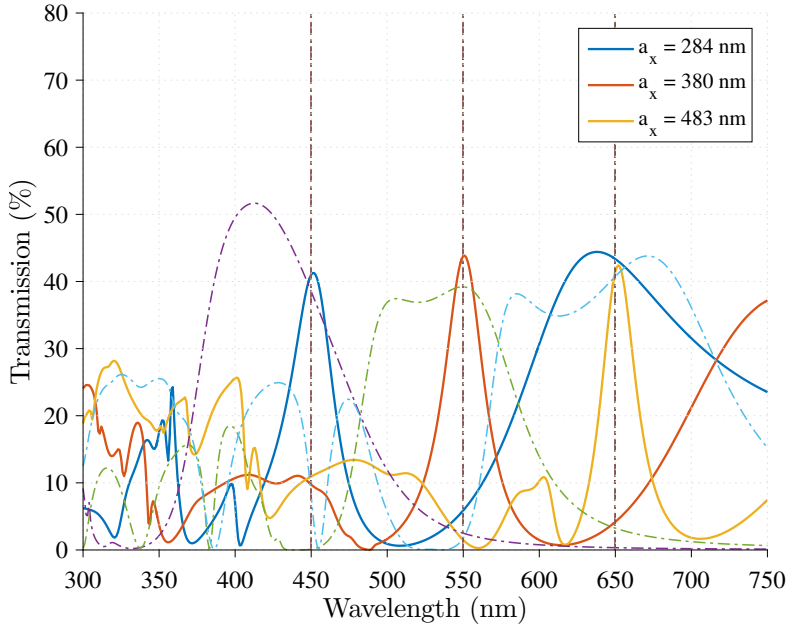

Figure 8: Optical transmissions of 40-nm Al filters, having silicon nitride filling inside the holes and 100 nm silicon nitride cap layer, whose periodicities have been estimated analytically on the graph in Fig. 7 given the desired working wavelength of 450 nm, 550 nm and 650 nm, in comparison with the RGB 150-nm thick Al PCFs (dashed curves). The periodicity to diameter ratio used is 1.8, which ensure the accuracy of the analytical method.

4. CONCLUSION

In this paper is has been shown that plasmonic colour filters can have FWHM of the order of 30 nm and transmission efficiency above 40% by changing the dielectric environment of the nanostructure. Moreover, the results that have been obtained show that it is not necessary to have a symmetric structure to ensure good coupling between the SPPs at the top and bottom interfaces and hence a relatively high transmission efficiency. Furthermore, the structure presented displays the same transmission characteristics at every wavelength of the visible spectrum, which means that the same total thickness can be used for all filters and the structure can be fabricated in a single lithographic step.

Clearly, this type of structure requires more optimization to be used as RGB filters on top of a photodetector or, alternatively, very good digital image processing performed in order to reduce/eliminate high cross-talk at longer wavelengths. Alternatively, this type of structure might be used as a subtractive filter. For example, in Fig. 8, the optical transmission for $a_x = 240$ nm is above 40% and approximately equal for wavelengths in the red and blue regions of the spectrum, while being almost zero in the green one, which means that this structure could be used as a magenta filter. Despite the need of optimization, this structure might open the doors to future multispectral detection with PCFs given the possibility to have a 10-nm resolution distance between a peak and the next one by varying the periodicity of the structure in 10-nm steps.

An analytical method to evaluate the periodicity, given a desirable working wavelength, has also been proposed for a 40-nm Al film with holes filled with silicon nitride and a 100-nm thick silicon nitride cap layer. The high accuracy of the method has been demonstrated and a further revision of the method through the integration of e.g. the silicon nitride thickness as a variable could make it work for designs with different structural parameters.

ACKNOWLEDGMENTS

N.P. would like to acknowledge the financial support of the European Commission, under the ITN Marie-Curie action (European Industrial Doctorate - Project reference: EDISON-GA).

APPENDIX A. SPPS PENETRATION DEPTH

Accordingly to the definition of SPPs, these surface waves show evanescent fields penetrating into both sides of the interface, i.e. into both the dielectric and the metal. The penetration depth into the dielectric δ_d and the penetration depth into the metal δ_m are given by:[15]

$$\delta_d = \frac{1}{k_0}\left|\frac{\epsilon_d + \epsilon_m}{-\epsilon_d^2}\right|^{\frac{1}{2}} \tag{7}$$

$$\delta_m = \frac{1}{k_0}\left|\frac{\epsilon_d + \epsilon_m}{-\epsilon_m^2}\right|^{\frac{1}{2}} \tag{8}$$

Fig. 9 displays the penetration depths into aluminium and silicon dioxide for the SPPs generated at an Al/SiO_2 interface, and the penetration depths into aluminium and silicon nitride for the SPPs generated at an Al/Si_3N_4 interface.

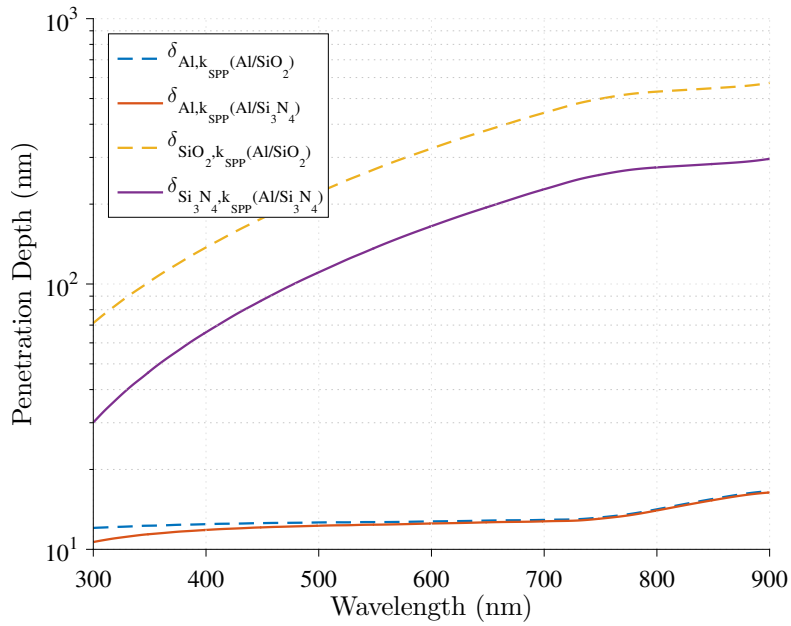

Figure 9: Penetration depths into aluminium and silicon dioxide for the SPPs generated at an Al/SiO_2 interface, and the penetration depths into aluminium and silicon nitride for the SPPs generated at an Al/Si_3N_4 interface.

REFERENCES

[1] Ebbesen, T. W., Lezec, H. J., Ghaemi, H. F., Thio, T., and Wolff, P. A., "Extraordinary optical transmission through sub-wavelength hole arrays," *Nature* **391**(6668), 667–669 (1998).

[2] Genet, C. and Ebbesen, T. W., "Light in tiny holes," *Nature* **445**(7123), 39–46 (2007).

[3] Catrysse, P. B. and Wandell, B. A., "Integrated color pixels in 018-Âţm complementary metal oxide semiconductor technology," *J. Opt. Soc. Am. A* **20**(12), 2293 (2003).

[4] Chen, Q., Chitnis, D., Walls, K., Drysdale, T. D., Collins, S., and Cumming, D. R. S., "CMOS Photodetectors Integrated With Plasmonic Color Filters," *IEEE Photonics Technol. Lett.* **24**(3), 197–199 (2012).

[5] Burgos, S. P., Yokogawa, S., and Atwater, H. A., "Color Imaging via Nearest Neighbor Hole Coupling in Plasmonic Color Filters Integrated onto a Complementary Metal-Oxide Semiconductor Image Sensor," *ACS Nano* **7**(11), 10038–10047 (2013).

[6] Palanchoke, U., Boutami, S., and Hazart, J., "CMOS-compatible metallic nanostructures for visible and infrared filtering," in [*Proc. SPIE*], Adibi, A., Lin, S.-Y., and Scherer, A., eds., **8994**, 89940Y–1 (2014).

[7] McCrindle, I. J. H., Grant, J., Drysdale, T. D., and Cumming, D. R. S., "Hybridization of optical plasmonics with terahertz metamaterials to create multi-spectral filters," *Opt. Express* **21**(16), 19142 (2013).

[8] Zeng, B., Gao, Y., and Bartoli, F. J., "Ultrathin Nanostructured Metals for Highly Transmissive Plasmonic Subtractive Color Filters," *Sci. Rep.* **3**, 2840 (2013).

[9] Shrestha, V. R., Lee, S.-S., Kim, E.-S., and Choi, D.-Y., "Aluminum Plasmonics Based Highly Transmissive Polarization-Independent Subtractive Color Filters Exploiting a Nanopatch Array," *Nano Lett.* **14**(11), 6672–6678 (2014).

[10] Yu, Y., Chen, Q., Wen, L., Hu, X., and Zhang, H.-F., "Spatial optical crosstalk in CMOS image sensors integrated with plasmonic color filters," *Opt. Express* **23**(17), 21994 (2015).

[11] "UV/VIS Bandpass & Laser Line Filters - Part no: FB450-40, FB550-40, FB650-40." http://www.thorlabs.de/newgrouppage9.cfm?objectgroup_id=1001.

[12] Pacifici, D., Lezec, H. J., Sweatlock, L. A., Walters, R. J., and Atwater, H. A., "Universal optical transmission features in periodic and quasiperiodic hole arrays," *Opt. Express* **16**(12), 9222 (2008).

[13] Chen, Q. and Cumming, D. R. S., "High transmission and low color cross-talk plasmonic color filters using triangular-lattice hole arrays in aluminum films," *Opt. Express* **18**(13), 14056–14062 (2010).

[14] Xingjie, N., Zhengtong, L., and V., K. A., "PhotonicsDB: Optical Constants." https://nanohub.org/resources/PhotonicsDB.

[15] Zhang, J., Zhang, L., and Xu, W., "Surface plasmon polaritons: physics and applications," *J. Phys. D. Appl. Phys.* **45**(11) (2012).